Accepted Manuscript

Towards “Precision Mining” of wastewater: Selective recovery of Cu from acid mine drainage onto diatomite supported nanoscale zerovalent iron particles

R.A. Crane, D.J. Sapsford

PII: S0045-6535(18)30450-8

DOI: 10.1016/j.chemosphere.2018.03.042

Reference: CHEM 20986

To appear in: *ECSN*

Received Date: 3 November 2017

Revised Date: 2 March 2018

Accepted Date: 5 March 2018

Please cite this article as: Crane, R.A., Sapsford, D.J., Towards “Precision Mining” of wastewater: Selective recovery of Cu from acid mine drainage onto diatomite supported nanoscale zerovalent iron particles, *Chemosphere* (2018), doi: 10.1016/j.chemosphere.2018.03.042.

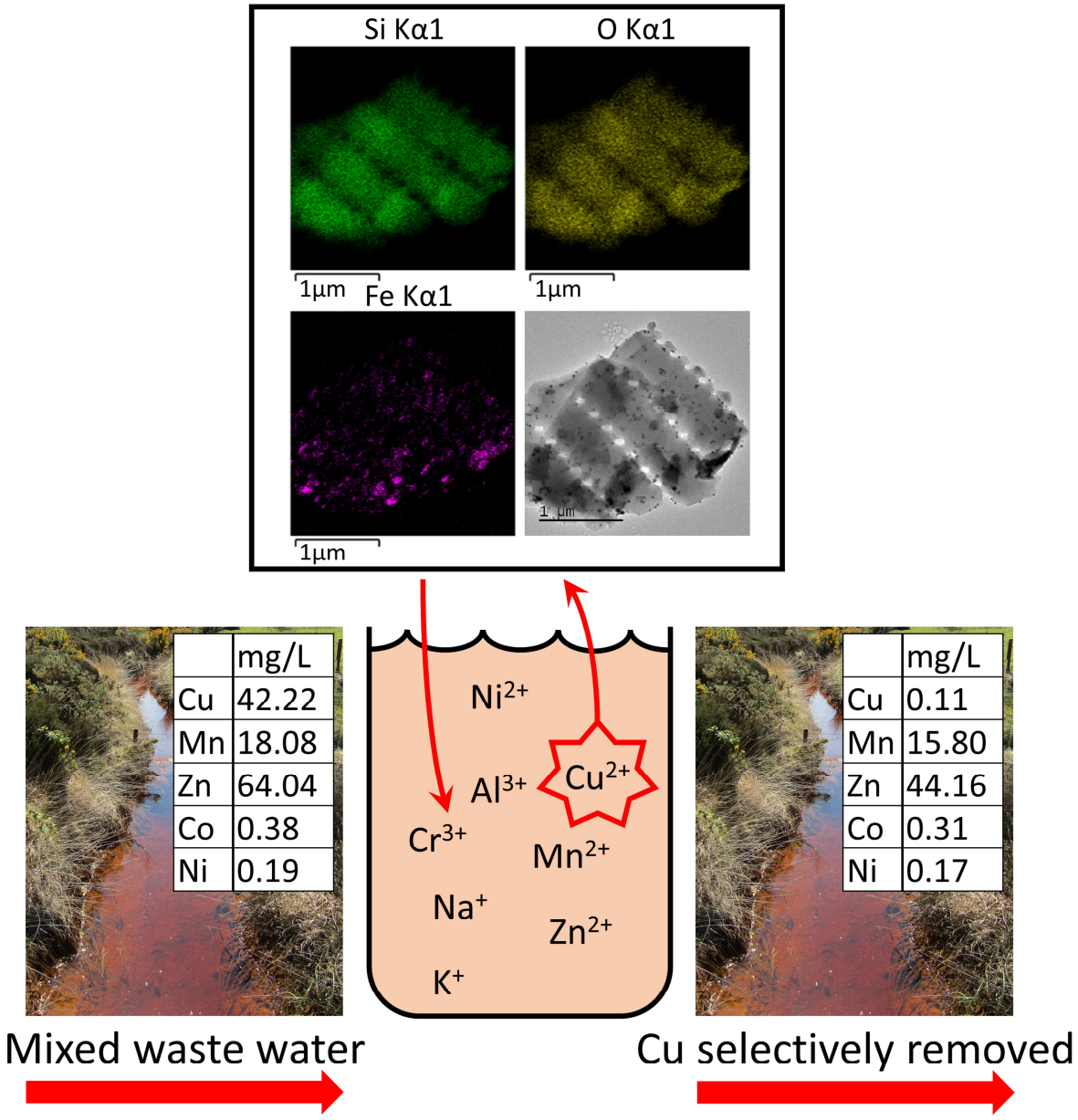
Si Kα1
O Kα1
1μm
1μm
Fe Kα1
1μm
1 μm
1μm
mg/L
Cu 42.22
Mn 18.08
Zn 64.04
Co 0.38
Ni 0.19
Ni2+
Al3+
Cu2+
Cr3+
Mn2+
Na+
Zn2+
K+
mg/L
Cu 0.11
Mn 15.80
Zn 44.16
Co 0.31
Ni 0.17
Mixed waste water
Cu selectively removed

Towards "Precision Mining" of wastewater: selective recovery of Cu from acid mine drainage onto diatomite supported nanoscale zerovalent iron particles

R. A. Crane[1]** *and D. J. Sapsford*[2]

[1] Camborne School of Mines, University of Exeter, Penryn Campus, Penryn, Cornwall, TR10 9FE. United Kingdom

[2] School of Engineering, Cardiff University, Queen's Building, The Parade, Cardiff, CF24 3AA. United Kingdom

* Corresponding author: r.crane@exeter.ac.uk

Key words: future mining, diatom, nanoparticles, nanocomposite, cementation, remediation

Abstract

This paper introduces the concept of 'Precision Mining' of metals which can be defined as a process for the selective *in situ* uptake of a metal from a material or media, with subsequent retrieval and recovery of the target metal. In order to demonstrate this concept nanoscale zerovalent iron (nZVI) was loaded onto diatomaceous earth (DE) and tested for the selective uptake of Cu from acid mine drainage (AMD) and subsequent release. Batch experiments were conducted using the AMD and nZVI-DE at 4.0-16.0 g/L. Results demonstrate nZVI-DE as highly selective for Cu removal with >99 % uptake recorded after 0.25 hours when using nZVI-DE concentrations ≥12.0 g/L, despite appreciable concentrations of numerous other metals in the AMD, namely: Co, Ni, Mn and Zn. Cu uptake was maintained in excess of 4 and 24 hrs when using nZVI-DE concentrations of 12.0 and 16.0 g/L respectively. Near-total Cu release from the nZVI-DE was then recorded and attributed to the depletion of the nZVI component and the subsequent Eh, DO and pH recovery. This novel Cu uptake and release mechanism, once appropriately engineered, holds great promise as a novel 'Precision Mining' process for the rapid and selective Cu recovery from acidic wastewater, process effluents and leach liquors.

Introduction

It is widely acknowledged that satisfying the projected future demand for metals requires innovations that will enable their recovery from hard to access ore deposits, as well as technospheric deposits and waste streams such as sludge residues, effluents and wastewater (Krook and Baas, 2013). Challenges arise for the exploitation of such ores, wastes and effluents including low grades/concentrations, and in some cases physical inaccessibility. This is also set within the context of the more rigorous environmental standards demanded for industrial processes, including the need to manage both solid and aqueous wastes.

As such it is clear that new paradigms for mining such new environments are urgently required. One such novel research arena is what we introduce here as 'Precision Mining' which pertains to the application of a methodology for the *in situ* selective recovery of a resource (e.g. a metal) from a deposit or material stream. The term has been taken by analogy from other industries which are currently undergoing 'precision' revolutions (e.g. Precision Medicine and Precision Agriculture). For example, Precision Medicine comprises a new rationale whereby a targeted approach to the delivery and release of therapeutic drugs within the body is applied, i.e. rather than treating the whole body with a large quantity of indiscriminate medicine (Hodson 2016). We see parallels here with a wide range of conventional mining and waste recycling techniques where the target chemical or metal/metalloid are often indiscriminately recovered with other elements, which leads to lengthy (and costly) further purification processes, which in turn will generate further wastes and associated negative environmental impact. Moreover, when selective metal (or metalloid) recovery methods are employed (e.g. using ion exchange resins) they are invariably applied *via ex situ* methods, such as pump-and-treat. In contrast the Precision Mining approach would

act to selectively recover the target metal *directly* from the ore body or waste stream (i.e. using an *in situ* technique) with minimal (or ideally zero) disturbance and/or associated waste products.

There are a number of combinations of materials and methods that could be envisaged to be used in different Precision Mining scenarios. One mechanism which holds great promise is the use of Fe^0 for the selective recovery of aqueous Cu *via* electrochemical cementation. Indeed previous work has determined nanoscale zerovalent iron (nZVI) as highly effective for the rapid and selective recovery of Cu from the aqueous phase (e.g. Scott et al., 2011). An intrinsic technical challenge associated with the use of nZVI (and other reactive nanomaterials) for water treatment, however, is their strong tendency to agglomerate due to van der Waals and/or magnetic attraction forces, which can considerably impact their aqueous reactivity and ability to behave as a colloid (Crane and Scott., 2012; Crane and Scott 2014; Scott et al., 2010; Noubactep et al., 2012). In order to overcome this limitation two main approaches have been adopted. The first uses surfactants, or other surface amendments, to increase the repulsive forces between the nanoparticles (e.g. Popescu et al., 2013). This method has been applied at various scales (up to field scale) and its major limitation is that the surface amendment often isolates or interferes with the ability of nZVI to react with aqueous contaminants (Crane and Scott., 2012). Another approach is to immobilise the nanomaterial onto a matrix support, which also has the additional benefit of curtailing concerns regarding the escape of nanomaterials into the environment. To date several different types of supports for nZVI have been investigated including bentonite (Xi et al., 2011), porous silica (Oh et al., 2007; Qiu et al., 2011), zeolite (Lee et al., 2007) and porous carbon (Crane and Scott., 2014; Lv et al., 2011). One disadvantage of such materials, however, is that their application is often limited as a fixed bed filter. In contrast nanocomposite materials which can be suspended in the aqueous phase as a colloid have a

much broader range of potential applications including those where the nanocomposite material can be injected into the subsurface for the *in situ* treatment (and if appropriate recovery) of target metals from contaminant plumes or leached ore bodies (Crane and Scott., 2012).

In this paper we have chosen to examine nZVI loaded onto diatomaceous earth (DE) for the Precision Mining (selective recovery) of Cu from AMD. DE deposits are found in numerous locations worldwide and are currently used as a low cost material in a wide range of products including as a mechanical insecticide, mild abrasive, absorbent for liquids and a reinforcing filler in plastics and rubber (Round et al., 1990). A highly beneficial attribute of DE is that it is a natural material, and as such likely to be more environmentally compatible than a similar material which is artificial in origin. Indeed the necessity for the use of environmentally compatible materials in Precision Mining is another area whereby there are likely to be similarities with Precision Medicine. In particular DE has received an increasing level of interest from researchers in recent years for its potential use as a next generation biocompatible drug delivery agent (e.g. as a magnetically guided drug microcarrier) (Chao et al., 2014). It is argued that by using this 'biotemplating' approach DE can provide many biomimetic advantages over conventional drug delivery platforms (Sarikaya 1999). It is anticipated that a similar benefit could be realised by using DE in Precision Mining, where there is also a fundamental necessity to use materials and methods which have minimal detrimental impact on the natural environment. In addition, the micron and submicron scale dimensions of diatoms and their subsequent ability to behave as a colloid enables extremely versatile nZVI-DE application. For example, nZVI-DE could be directly injected into porous media (e.g. a metal-rich plume in the subsurface) using technology that is similar to what is currently applied for the injection of nZVI into the subsurface for remediation applications

(Crane and Scott 2012), with the nZVI-DE then in theory recovered using cross-bore extraction or, if appropriate, a magnetic field.

This work has been established in order to investigate the fundamental behaviour of nZVI-DE for the selective recovery of Cu from AMD. Very little is currently known on this topic, with only a few studies currently in the literature (e.g. Sheng et al., 2016; Pojananukij et al., 2016; Pojananukij et al., 2017). To the best of our knowledge no studies have yet examined the application of nZVI-DE for the removal of aqueous Cu nor have any studies investigated the use of nZVI-DE for the recovery of metals or metalloids from "real" (i.e. non-synthetic) water. This study has been established in order to bridge this gap in our understanding and investigate whether nZVI-DE could be applied for the Precision Mining of Cu from AMD, which is one of the most prominent environmental issues currently facing the mining industry, and regarded by the European Environment Bureau and the US Environmental Protection Agency as rated "second only to global warming and stratospheric ozone depletion in terms of global ecological risk" (European Environment Bureau., 2000).

2. Materials and methods

2.1. AMD sampling location

The AMD was collected from Parys Mountain which is a disused open cast Cu-Pb-Zn mine on Anglesey (Wales, UK) (Kay et al., 2013). The AMD discharging from the Parys Mountain site is acidic (pH generally <3) and metal and metalloid-rich due to the oxidation of sulphide minerals. The geology and ore mineralogy of the site have been described by Pointon and Ixer (1980), with the AMD (and associated heavy metals) likely derived from pyrite, chalcopyrite, sphalerite and galena, amongst others. AMD samples were collected from the Duffryn Adda adit at GPS location: 53°23'40.96 N, 4°21'01.80 W. Samples were sealed in

high-density polyethylene bottles (without headspace) and stored at 4°C until required (maximum storage time was 7 days).

2.2. nZVI-DE synthesis

The DE (Holistic Detox Ltd, B0083HO2MY) was first acid washed using 1M HCl at a 1:10 solid liquid (SL) ratio for 2 hrs under constant agitation (150 RPM). The acid washed DE slurry was then centrifuged at 3077 *g* (4000 rpm) for 240 s and the supernatant was decanted. Milli-Q water (>18.2 MΩ cm) was then added to the DE at a 1:10 SL ratio and then gentle agitated. The slurry was then centrifuged at 3077 *g* for 240 s and the supernatant was decanted. The process was then repeated twice more. The DE was then dried in an oven for 48 hrs at 80'C. 10 g of $FeCl_2.H_2O$ was added to a mixture of 150 mL of absolute ethanol (Fisher Scientific, 12478730) and 50 mL of Milli-Q. The Milli-Q water ethanol mixture was first purged using N_2 gas for 30 mins. 10 g of the DE was then added and the slurry was stirred for 24 hrs (150 RPM) using a Stuart SSL1 orbital shaker table. The slurry was then centrifuged at 3077 *g* for 240 s and the supernatant decanted. 400mL of a 0.8 M $NaBH_4$ solution was then added dropwise. The suspension was then agitated for 30 minutes at 150 RPM. The suspension was then centrifuged at 3077 *g* for 240 s and the supernatant was decanted. Absolute ethanol was then added at a 1:10 SL ratio and then gently agitated. The suspension was then centrifuged at 3077 *g* for 240 s and the supernatant was decanted. This was repeated twice more. The resultant nZVI-DE was then dried in a vacuum desiccator (approx. 10^{-2} mbar) for 72 h and then stored in an argon filled (BOC, 99.998%) MBraun glovebox until required.

2.3. Batch experiments

Prior to conducting any batch experiments to investigate the exposure of nZVI-DE to AMD, the AMD was removed from the refrigerator and allowed to equilibrate in the ambient

laboratory (temperature = 20 ±0.5°C) for 24 hrs. Unless specified differently all batch systems comprised 200 mL volume of the AMD in 250 mL clear soda lime glass jars (Fisher Scientific, 11704329). Following nZVI-DE addition each batch system was sealed (using the jars screw cap) and placed on the benchtop in the open laboratory. Periodic sampling of dissolved oxygen (DO), oxygen reduction potential (ORP) and pH was conducted by gently agitating each batch system in order to ensure homogeneity. The pH, Eh and DO probes were calibrated prior to each measurement. The measured Eh values were converted to Eh standard hydrogen electrode by subtracting the difference between the measured Eh of the reference solution (220mV ±5) with the true Eh of the reference solution (Mettler Toledo 220 mV/pH 7 reference solution). 5 mL aqueous-nZVI suspensions were periodically taken using an auto-pipette. The extracted suspensions were centrifuged at 4000 RPM (3077 *g*) for 240 seconds after which the supernatant became clear (i.e. all of the nZVI was centrifuged to the bottom of the vial). The supernatant was then extracted using a 10 mL syringe and filtered through a cellulose acetate filter 0.2 µm filter. The filtrate was prepared for inductively coupled plasma mass spectrometry (ICP-MS) analysis by the additional of HNO_3 at a concentration of 2 % by volume. The solid nZVI-DE plug at the base of the centrifuge vial was prepared for X-ray diffraction (XRD) and high resolution transmission electron microscopy (HRTEM) by an absolute ethanol wash. This was conducted by adding 20 mL of the ethanol (Fisher Scientific, 12478730) and then gently agitating the centrifuge vial in order to suspend the nZVI-DE plug. The vial was then centrifuged at 4000 RPM (3077 *g*) for 240 seconds in order to separate the solid and aqueous phases. The supernatant was then removed and the process was repeated a further two times. Each time the supernatant was decanted the nZVI-DE plug at the bottom of the centrifuge vial was maintained in place using an Eclipse 20mm Neodymium Pot Magnet (length 25mm, pull force 28kg). Once the ethanol washing process was completed the nZVI-DE plug was pipetted onto a glass optical microscope slide (Agar

Scientific, G251P) and a Au coated holey carbon film (TAAB, C062/G) for XRD and HRTEM analysis respectively. Samples were then dried in a vacuum chamber at $<1 \times 10^{-2}$ mbar for a minimum of 2 h prior to analysis. All sorption-desorption experiments were conducted at room temperature (measured to be 20.0°C ±1.0°C) and ran as duplicate pairs, with the average data used to create the figures/tables displayed herein.

2.4. Analysis techniques

Each powder sample was prepared for ICP-OES analysis *via* a 4 acid digest (EPA 1996). Firstly, 0.01 g was placed in a PTFE lined microwave digest cell and 3 mL of analytical grade 45.71% hydrofluoric acid (HF) was then added and left for 12 hrs. 6 mL of aqua regia solution (1:1 ratio of analytical grade 32% hydrochloric acid (HCl) and 70 % nitric acid (HNO_3)) was then added and the container was then placed in a microwave digest oven (Anton Paar Multiwave 3000) and heated at 200°C (1400 watts) for 30 minutes (after a 10 minute up ramp time period) and then allowed to cool for 15 minutes. The resultant solution was then neutralised using 18 mL of analytical grade 4 % Boric acid (H_3BO_3) at 150°C (900 watts) for 20 minutes (after a 5 minute up ramp time period) and then allowed to cool for 15 minutes. ICP-OES analysis was performed using a Perkin Elmer Optima 2100 DV ICP-OES. ICP-MS was performed using a Thermo X Series 2 ICP-MS. A Phillips Xpert Pro diffractometer with a CoKa radiation source was used for XRD analysis (generator voltage of 40 keV; tube current of 30 mA). XRD spectra were acquired between 2h angles of 10–90 °, with a step size of 0.02° 2 and a 2 s dwell time. BET surface area analysis was performed using a Quantachrome NOVA 1200 surface area analyser, with N2 as the adsorbent and following a 7 point BET method. Prior to analysis the samples were degassed under vacuum (∼10−2 mbar) for a 24 h period at a temperature of 75 °C. Samples were ran as triplicates with the average recorded. HRTEM analysis was performed using a JEOL JEM-2100 microscope at 200 kV. Energy dispersive spectroscopy (EDS) analysis and mapping was

performed using Oxford Instruments X-MaxN analyzer and Aztec software. A beryllium sample holder was used in order to prevent any background Cu from being detected. X-ray photoelectron spectroscopy (XPS) spectra were collected using a Thermo K-Alpha+ spectrometer. Spectra were collected at a pass energy of 40 eV for narrow scans and 150 eV for survey scans with a 0.1 and 1 eV step respectively. Charge neutralisation was achieved using a combination of low energy electrons and argon ions. Spectra were quantified in CasaXPS using Scofield sensitivity factors and an energy dependence of -0.6. In order to determine the relative proportions of Fe^{2+} and Fe^{3+} in the sample analysis volume, curve fitting of the recorded Fe $2p_{3/2}$ photoelectron peaks was performed following the method of Scott et al. (2005). The Fe $2p_{3/2}$ profile was fitted using photoelectron peaks at approximately 706.7, 709.1, 710.6 and 713.4 eV corresponding to Fe^0, Fe^{2+} octahedral; Fe^{3+} octahedral and Fe^{3+} tetrahedral. These parameters were selected on the basis that the surface oxide was assumed to be a mixture of w*ü*stite and magnetite, as the oxide Fe^{2+} is in the same coordination with the surrounding oxygen atoms in both forms of oxide. The particle size distribution (PSD) of the nZVI (within nZVI-DE) was measured using HRTEM images (ImageJ Java 1.6.0_24 software; 104 measurements were performed).

3. Results and discussion

3.1. Characterisation of the nZVI-DE

Characterisation of the DE and nZVI-DE was performed using BET surface area analysis, HRTEM, XRD, XPS and ICP-OES (following acid digestion), with the results summarised in Table 1. BET surface area analysis determined that the surface area of the DE was 29.7 m^2/g compared to 6.5 m^2/g recorded for the nZVI-DE, with the lower surface area of the latter material attributed to agglomeration of the material (which was also observed visually).

HRTEM analysis determined that the DE comprised Si bearing frustules of various shapes and sizes in addition to a minor component of fragmented Si bearing material, which were likely frustules which have been mechanically broken, with sizes ranging from submicron scale to hundreds of microns in diameter (Figure 1 and S1). In contrast to previous studies where nZVI have been recorded as typically arranged in chains and rings aggregates (due to magnetic and/or Van der Waals attraction) the nZVI within the nZVI-DE were typically recorded as individual particles adhered to the surface of the DE in a relatively even spacing (Figure 1). This suggests that each nZVI particle was likely to have formed directly upon the surface of the DE, i.e. as an ultra-small nanoparticle nuclei which then subsequently grew upon the DE surface into the final nZVI product. This observation also provides clear evidence that the nZVI within the nZVI-DE are relatively strongly bound to the DE (i.e. fixed in their position). Furthermore, no discrete nZVI were recorded upon the carbon coated TEM grid (i.e. all nZVI were recorded as attached to the DE). The nZVI particles upon the DE were determined to be spherical in shape, generally within a size range of 10-100 nm and an average diameter of 38.0 nm (Figure 1). Each individual nZVI particle was recorded to contain a discrete outermost layer (density contrast), which is attributed to be the presence of an oxide shell surrounding the Fe^0 core as previously recorded in other nZVI characterisation studies (e.g. Crane et al., 2015a; Crane et al., 2015b; Pullin et al., 2017). XRD determined the crystalline component of DE to be comprised of SiO_2 with well-defined peaks corresponding to SiO_2(101), SiO_2(011) and SiO_2(112) recorded (Figure 2). A similar XRD profile was recorded for the nZVI-DE except with an additional peak centred at 52.4° 2θ recorded and attributed to be the (110) lattice reflection of α-Fe^0 (Figure 2). Table 1 displays the concentration (wt. %) of notable metals present in the DE and nZVI-DE (following acid digestion). It can be observed that both materials largely comprised of Si with a minor component of Al. Fe was present in relatively minor concentrations within the DE (0.72 wt.

263 %) compared to 2.60 wt. % recorded for the nZVI-DE, which is attributed to the presence of
264 the nZVI. A higher concentration of Na was also recorded for the nZVI-DE and attributed to
265 residual $NaBH_4$ used in the nZVI synthesis. This corroborates with the surface composition
266 (at. %) data (Table 1) determined from XPS where concentrations of Na, B and Fe were all
267 higher for the nZVI-DE than the DE. XPS analysis determined the outer surface of the nZVI
268 (upon the DE) was comprised of a mixed valent (Fe^{2+}/Fe^{3+}) oxide overlying a Fe^0 core
269 (Figure 3). Given the mean free path of Fe is equivalent to approximately 6 atomic layers,
270 this detection of Fe^0 in the XPS analysis volume therefore indicates that the oxide thickness is
271 likely to be <5nm, which corroborates with the nZVI oxide thickness measurement using
272 HRTEM.

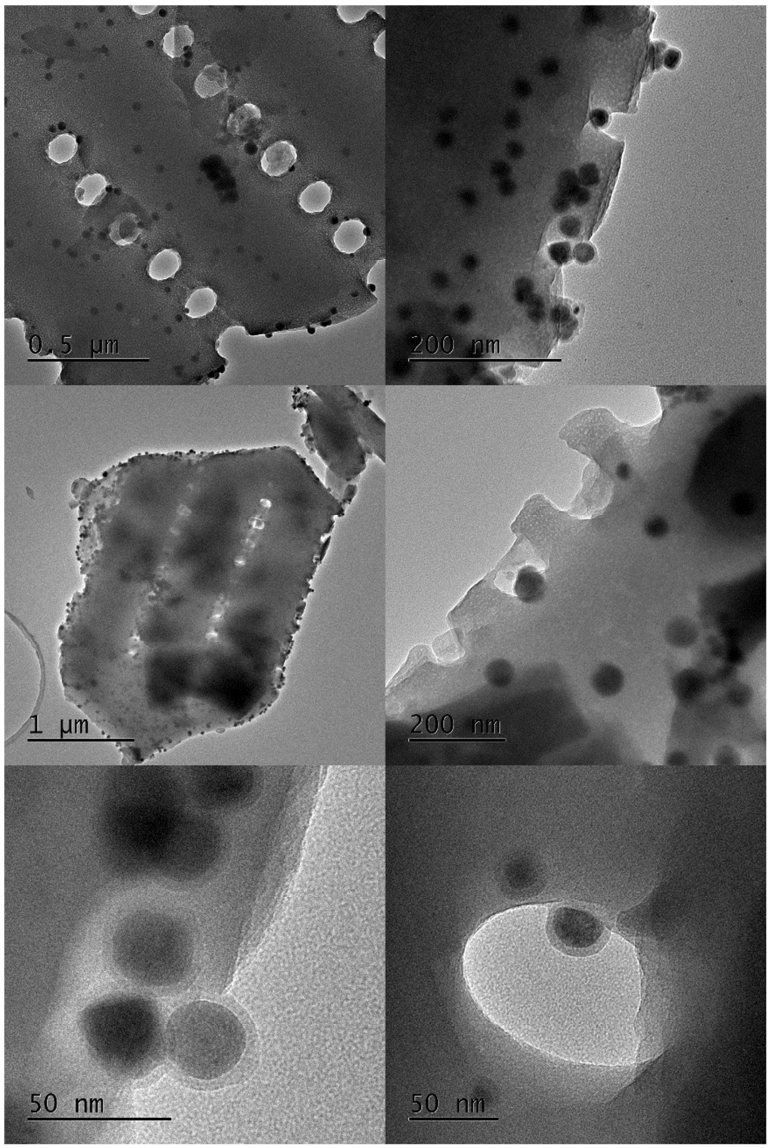

273

274 **Figure 1.** HRTEM images of the as-formed nZVI-DE

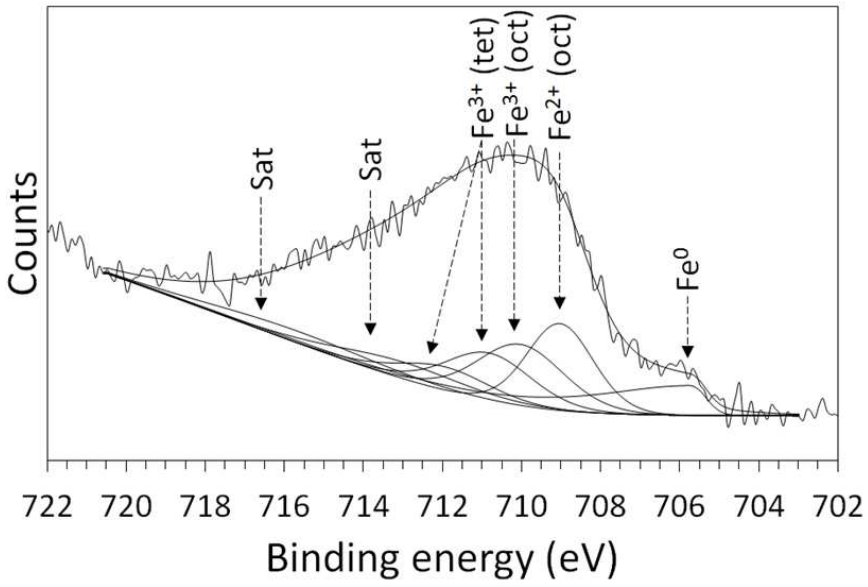

275

276 **Figure 2.** Curve fitted XPS Fe $2p_{3/2}$ photoelectron spectra for the nZVI-DE

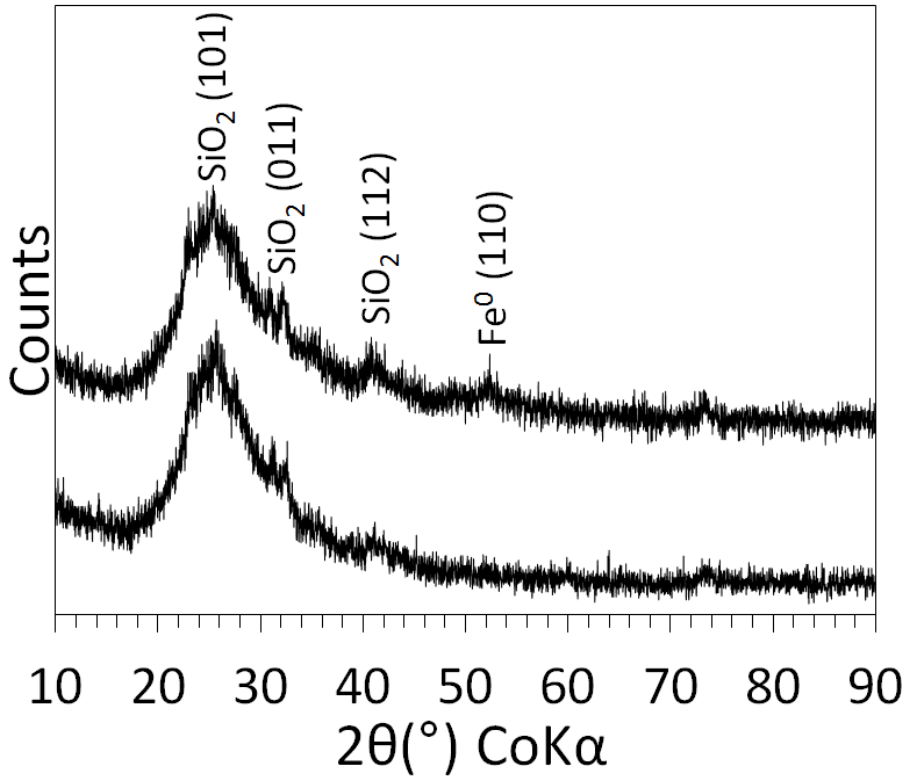

277

278 **Figure 3.** XRD profiles for the DE (bottom) and nZVI-DE (top).

279

280

281 **Table 1.** Summary of the physicochemical properties of the DE and nZVI-DE. *Average
282 diameter and PSD measurements were not possible for the DE due to their anisotropic shape
283 **ICP-OES analysis was performed on DE and nZVI-DE following their digestion in HF,
284 NaOH, HCl and H_3BO_3 (see Section 2.1.). Note: Zn, Mn, Cr, Cu, Pb, Ni, Sb, Li and Mo were
285 also analysed but recorded as at concentrations below the detection limit of the ICP-OES
286 instrument.

Parameter	Analysis technique	Subparameter	DE	nZVI-DE
Bulk composition	XRD	n/a	SiO_2	SiO_2, α-Fe^0
nZVI average diameter (nm)	HRTEM*	n/a	n/a	38.0
nZVI PSD (%)	HRTEM*	0-50 nm	n/a	71.1
		50-100 nm	n/a	28.9
		>100nm	n/a	0.0
Surface composition (at. %)	XPS	Al 2p	3.1	2.0
		C 1s	6.5	19.2
		K 2p	0.2	0.0
		Cl 2p	0.9	0.7
		Fe 2p3/2	0.5	1.4
		O 1s	59.4	47.9
		Si 2p	29.4	16.6
		B 1s	0.0	4.6
		Na 1s	0.0	7.6
Bulk composition (wt. %)	ICP-OES**	Al	1.67	1.33
		K	0.33	0.25

		Ca	0.14	0.10
		Fe	0.72	2.60
		Ti	0.10	0.08
		Na	0.21	3.19
		Mg	0.22	0.14
		Si	38.69	33.97
		Sn	0.01	0.01
		S	0.05	0.05
		W	0.01	0.01
Fe stoichiometry ($Fe^0/Fe^{2+}+Fe^{3+}$)	XPS	n/a	n/a	0.20
Fe stoichiometry (Fe^{2+}/Fe^{3+})	XPS	n/a	n/a	0.49
Specific surface area (m^2/g)	BET	n/a	29.7	8.5

3.2. Characterisation of the AMD

Prior to nZVI-DE addition the pH, Eh and dissolved oxygen (DO) of the AMD was measured along with the concentrations of dissolved metals and metalloids using ICP-MS. The water was acidic (pH = 2.67) and oxygenated (Eh and DO recorded to be 490 mV and 8.98 mg/L respectively). The levels of contamination in the AMD are demonstrated through comparison with WHO recommended drinking water human health guideline concentrations (WHO 2011), Table 2 to emphasise the extent of contamination. Several elements were recorded as exceeding the guideline concentrations, namely Mn, Ni, Cu, Cd, As and Pb by factors of 45.2, 2.8, 21.1, 56.0, 27.7 and 1.8 respectively. The concentrations of all metals and metalloids analysed using ICP-MS is displayed in Table S1.

3.3. Changes in pH, Eh and DO following nZVI-DE addition

The addition of the nZVI-DE to all batch systems containing AMD resulted in a rapid decrease in Eh and DO and a concurrent increase in pH (Figure S2). Most significant change was recorded for the batch systems containing the largest concentration of nZVI-DE with only relatively minor changes recorded for the batch systems containing nZVI-DE at <4.0 g/L. Eh minima occurred for all systems within the first four hours of reaction, with 430, 112, -337 and -412 mV recorded for systems containing nZVI-DE at concentrations of 4.0, 8.0, 12.0, 16.0 g/L respectively. Maximum pH also occurred within the first four hours of reaction for all systems, with 2.92, 4.31, 5.64 and 6.28 recorded for batch systems containing nZVI-DE at concentrations of 4.0, 8.0, 12.0, 16.0 g/L respectively. This behaviour is attributed to the rapid oxidation of the nZVI surfaces during their initial exposure to the AMD, consuming DO and H^+ and reducing the Eh of the system. Following this initial reaction period gradual reversal to pH, Eh and DO conditions that were similar to pre-nZVI-DE exposure was observed in all systems, which is attributed to the reactive exhaustion of the nZVI (i.e. total transformation of Fe^0 to quasi-stable Fe^{2+} and/or Fe^{3+} (hydr)oxide products).

3.4. Changes in metal and metalloid concentrations following nZVI-DE addition

The addition of the nZVI-DE to the AMD resulted in significant changes in the aqueous concentration of several different metals and metalloids (Figure 4 and Table 2). The most significant concentration decreases were recorded for Cu, Cd, As and Pb with removal of these metals to ≤2.5 µg/L recorded within 1 hr reaction time, when using a nZVI-DE concentration of 16.0 g/L, followed by retention at very low levels (as indicated by comparison to WHO specified drinking water guideline concentrations, Table 2) for time periods of 24, 2, 336 and 672 hrs for Cu, Cd, As and Pb respectively. A minor decrease in the concentrations of Mn, Zn and Ni was also recorded.

It is widely accepted that when nZVI is synthesised in the open laboratory (i.e. not under an inert atmosphere) *via* the chemical reduction of aqueous $Fe^{2+}_{(aq)}$ it gains a surface oxide layer directly after synthesis. However, the thin and disordered nature of this oxide is known to enable electron passage (*via* tunnelling or through defect sites) and thereby conserve the reducing capability of Fe^0. As such it is relevant to refer to standard electrode potentials for the reduction of cationic metals and metalloids in comparison to that of Fe ($Fe^{2+}_{(aq)} + 2e^- \rightarrow Fe^0_{(s)}$ E^0 = -0.44 V) in order to determine their likely removal mechanism onto nZVI. In particular it is likely that the removal of Cu and Pb recorded by the nZVI-DE is likely to have been *via* chemical reduction (Xi et al., 2010), because the E^0 for the reduction of their divalent cations to a metallic state is 0.34 and -0.13 V respectively. Indeed the reduction of aqueous mono- or divalent Cu to Cu^0 using zero-valent metals lower on the galvanic series such as Fe^0, Zn^0, Al^0 (termed "cementation") has been used extensively exploited in hydrometallurgical processes for Cu recovery. Ni^{2+} and Cd^{2+} exhibit E^0 which are only slightly more electropositive than Fe^0 and as such their likely removal mechanism by nZVI-DE was *via* a combination of chemical reduction at the nZVI surface and adsorption onto nZVI corrosion products. Similarly, it is likely that As removal recorded herein was likely to have been *via* a combination of sorption (onto nZVI corrosion products) and chemical reduction upon the nZVI, however, other studies have also documented simultaneous oxidation of As compounds (e.g. $As^{3+} \rightarrow As^{5+}$) by iron oxides (Ramos et al., 2009). Partial removal of Zn onto the nZVI-DE was observed, however, despite the E^0 for the cathodic reduction of aqueous Zn^{2+} to its metallic state is -0.76 V, and therefore considerably lower than -0.44 V. As such Zn^{2+} is thermodynamically unlikely to have been chemically reduced by nZVI-DE with its removal instead likely to have been caused by the increase in pH, resulting in the co-precipitation (and adsorption) of Zn with iron corrosion products and/or iron (hydr)oxides derived from native iron within the AMD (Crane et al., 2015a). Minimal

concentration changes were determined for cations: K, Ca, Mg, and Mn (Table S2) which demonstrates that nZVI is selective for the removal of certain metals from solution (namely those whose solubility is redox sensitive). In general greater aqueous Fe concentrations were determined for the batch systems containing lower concentrations of nZVI-DE, which is in contrast to previous studies who have examined the exposure of nZVI to AMD where a positive correlation has been recorded (e.g. Crane and Scott 2014). The mechanism for this contrasting result is likely due to the higher pH in the batch systems containing higher nZVI-DE concentrations which in turn may have resulted in the precipitation and co-precipitation of Fe-bearing phases and thus the removal of Fe from the aqueous phase.

Whilst Cu and Cd were initially removed from solution they were subsequently found to redissolve in all batch systems studied. This behaviour is in agreement with other studies (e.g. Crane et al., 2011) and it attributed to the reactive exhaustion of the nZVI and consequent reversal of the solution chemistry to pre-nZVI-DE addition conditions, resulting in the oxidative dissolution and/or desorption of metals as pH reverted to lower values and Eh increased in response to oxygen ingress. In contrast, Fe concentrations in solution reflect the dynamics of both dissolution and precipitation reactions. Initial increases in concentration are due to the oxidative dissolution of Fe^0 and decreases a response to either increasing pH and Eh that ultimately lead to the precipitation of Fe(III) oxyhydroxides which are stable under ambient (starting) Eh/pH conditions. As such the lack of Fe redissolution recorded in the latter stages of the experiment suggests that such Fe was in a physicochemical form which was more resistant (than Cu and Cd) to acidic dissolution. Similarly the fact that both Cu and Cd were recorded to readily redissolve at acidic pH suggests that such metals were likely present as phases which were relatively susceptible to acidic dissolution.

372

373 **Table 2.** Notable contaminant metal and metalloids present in the AMD as analysed using
374 ICP-MS along with their WHO recommended drinking water health guideline concentrations
375 (WHO 2011). Metal/metalloid concentrations of the AMD following exposure to the nZVI-
376 DE after 0.25 hr as analysed using ICP-MS are also listed. Cells are coloured in red where
377 metal/metalloid concentrations exceed the WHO threshold.

Metal/metalloid	Concentration in AMD (mg/L)	WHO drinking water guideline concentrations (mg/L)	Concentration after 0.25 hr (nZVI-DE at 4.0 g/L)	Concentration after 0.25 hr (nZVI-DE at 8.0 g/L)	Concentration after 0.25 hr (nZVI-DE at 12.0 g/L)	Concentration after 0.25 hr (nZVI-DE at 16.0 g/L)
Mn	18.083	0.4	17.677	17.482	15.671	16.881
Ni	0.193	0.07	0.206	0.205	0.187	0.193
Cu	42.216	2	41.654	30.261	0.243	0.404
Zn	64.039	No limit	58.541	56.244	44.556	46.451
Cd	0.168	0.003	0.169	0.153	0.018	0.021
As	0.277	0.01	0.234	0.032	<DL	0.003
Pb	0.018	0.01	0.018	0.006	0.003	0.002

378

379

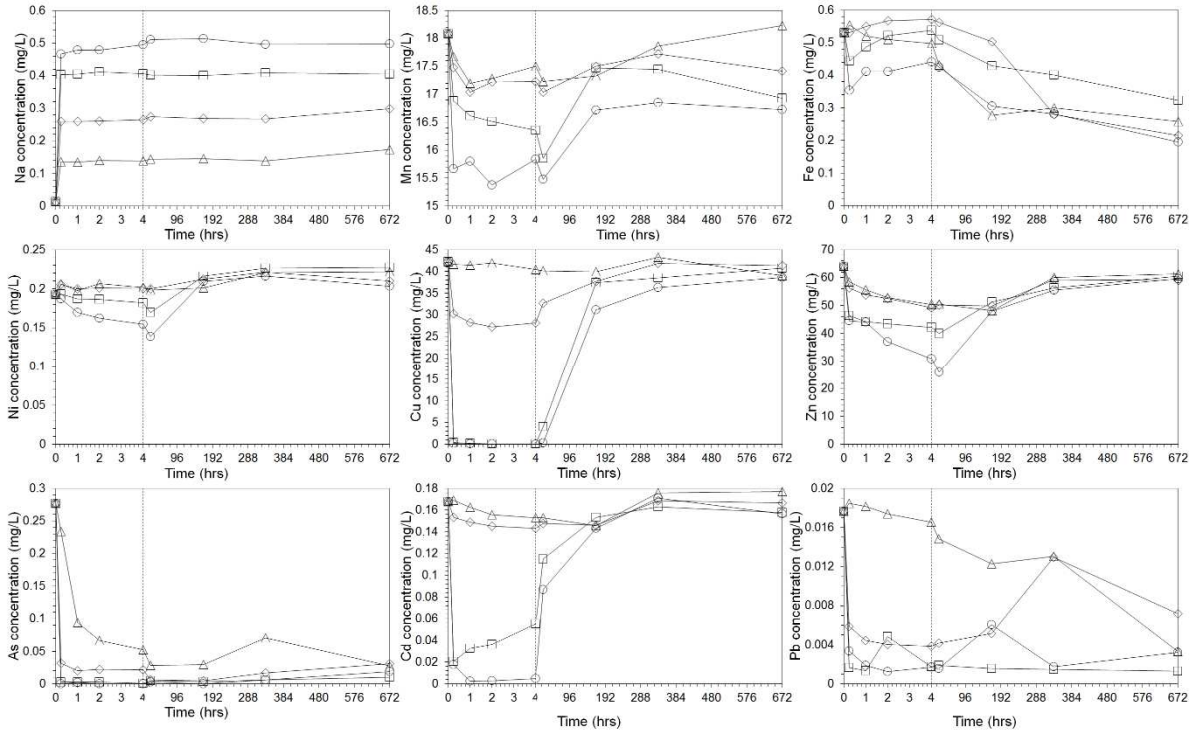

Figure 4. Aqueous concentrations of notable metal and metalloids as a function of time for the AMD when exposed to nZVI-DE at 4.0 (triangle markers), 8.0 (diamond markers), 12.0 (square markers) and 16.0 g/L (circle markers).

3.5. XRD analysis of nZVI-DE following exposure to the AMD

XRD was used to determine the bulk crystallinity and composition of nZVI-DE solids extracted from all batch systems at periodic time intervals during their exposure to the AMD (Figure S3). A rapid transition from a mixture of SiO_2 and Fe^0 (recorded for the as-formed nZVI-DE) to SiO_2 was recorded for all systems and attributed to the dissolution (i.e. aqueous corrosion) of the nZVI into the AMD. No sorbed phases (e.g. Cu^0) were detected, which was not expected given the relatively low concentration of metals and metalloids in the AMD and the % level detection limits typical of XRD.

3.6. HRTEM-EDS analysis of nZVI-DE following exposure to the AMD

Figure 5 displays HRTEM images and corresponding EDS maps for Si, O, Fe and Cu for the nZVI-DE extracted from the AMD water at periodic intervals. It can be observed that similar to the as-formed nZVI-DE (Figure 1), all nZVI were attached to the DE (i.e. no discrete nZVI were recorded upon the carbon coated TEM grid), which indicates that they were unlikely to have dettached from the DE during and throughout their exposure to the AMD. Si and O comprised the vast majority of the wt. % composition of the nZVI-DE, with only minor concentrations of Fe and Cu. Fe concentrations were lower than the as-formed nZVI-DE for the two samples taken from 1 and 4 hours exposure to the AMD and slightly higher for the sample taken from 672 hours (Table 3). This correlates well with the ICP-MS data (Figure 4) which shows an initial dissolution of Fe (from the nZVI-DE) during the initial stages of reaction (e.g. ≤24 hrs) followed by subsequent precipitation. The detection of Cu upon the nZVI-DE confirms that the removal of Cu ions from solution was a surface mediated process, however, no conclusive determination can be made for the specific Cu removal behaviour (e.g. preferential removal of the Cu ions onto nZVI than the DE) due to the low concentrations.

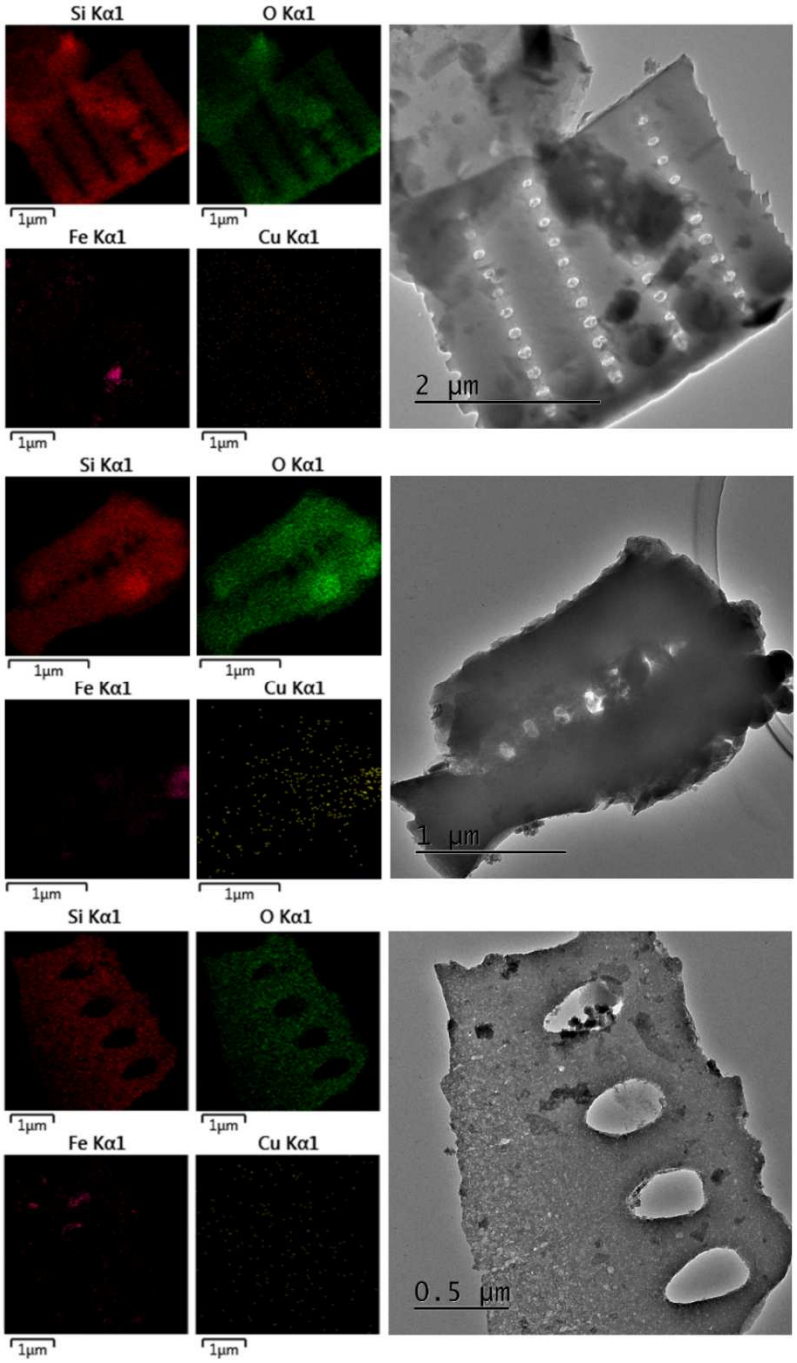

408

409 **Figure 5.** HRTEM images and corresponding EDS maps for Si, O, Fe and Cu for the nZVI-
410 DE extracted from the AMD water after 1, 4 and 672 hrs (stacked from top to bottom) when
411 using nZVI-DE concentrations of 16.0 g/L.

Table 3. Composition (by wt. %) of the nZVI-DE after exposure to the AMD after 1, 4 and 672 hrs as determined using HRTEM-EDS. The data correlate to the EDS maps displayed in Figure 5.

	1 hr	4 hrs	672 hrs
O	50.87	52.00	54.16
Na	0.16	0.26	0.00
Mg	0.06	0.20	0.00
Al	0.73	1.80	1.32
Si	47.21	41.57	42.38
S	0.00	0.63	0.00
K	0.09	0.10	0.00
Fe	0.84	3.33	2.12
Cu	0.03	0.12	0.02

4. Environmental/industrial implications

Herein we introduce Precision Mining as a new concept which can be defined as a methodology for selective *in situ* metal uptake from a material or media, with subsequent retrieval and recovery of the target metal with the benefits of minimal disturbance to all other components (metals, anions, microbiota, dissolved organic matter, hydro-geochemical conditions, etc.). There are a wide variety of (nano)material combinations that could be envisaged for uses in different Precision Mining scenarios, however, one particularly promising material, which has already received significant attention in Precision Medicine as a next generation biocompatible drug delivery agent, is DE. Its potential use in combination with nZVI as a Precision Mining tool for the removal of Cu from the aqueous phase has,

426 however, not been investigated until now. Results documented herein comprise initial data on
427 this topic and demonstrate that the material holds great promise as a next generation Precision
428 Mining tool for the rapid and selective recovery of Cu from wastewaters, such as AMD.

429 The benefits of using the DE as a carrier material (vehicle) for the reactive component are: (i)
430 it prevents agglomeration and subsequent passivation of the nZVI; (ii) it is off sufficiently
431 small size that a DE slurry is relatively easy to maintain and pump wherever it is needed; (iii)
432 it is an inexpensive commercially available material that is highly resistant to attack from
433 acidic wastewater, effluents and leach liquors.

434 The benefits of nZVI for Cu recovery from wastewaters are: (i) it is highly selective for the
435 recovery of Cu from acidic waters; and (ii) on return to ambient pH/Eh conditions the Cu is
436 spontaneously released back to the aqueous phase. In combination these attributes enables
437 nZVI-DE to be considered as a highly efficient and selective Precision Mining tool for the
438 recovery from Cu from wastewater. The latter is a particularly interesting phenomena and
439 enables the highly efficient concentration of Cu whereby following the selective recovery of
440 Cu from the acidic waste water the nanocomposite material can then be separated from the
441 target effluent (e.g. by centrifugation or coagulation/flocculation) and allowed to release the
442 Cu into a smaller volume, thus concentrating the Cu for final recovery. The nZVI-DE can
443 therefore be considered to be partially “self-regenerating” (although it would need to re-
444 loaded with fresh nZVI in order for reuse).

445 It is envisaged that the superparamagnetic properties of nZVI-DE could also enable efficient
446 transport and/or recovery of the nanomaterial, which is likely to unlock a wide range of
447 different potential applications for the nanomaterial (e.g. subsurface injection of nZVI-DE for
448 the *in situ* recovery of Cu from aqueous plumes, followed by magnetic recovery). Further
449 work is required in order to determine both the hydraulic (e.g. colloidal stability, dynamic

zeta potential) properties of the material and also its behaviour towards and within biological systems. Another important aspect to consider is the cost associated with the manufacture and application of nZVI-DE. Whilst DE is relatively cheap to source from primary deposits (typical cost can range from 100-400 USD/tonne (USGS 2012)) nZVI is much more expensive (e.g. 10-140 USD/kg, depending on the purity and quantity purchased (Crane and Scott 2012; Stefaniuk and Oleszczuk 2016)). However, very few companies currently exist which manufacture nZVI and as such this cost is likely to significantly decrease if demand for the nanomaterial increased in the future. An additional factor to consider is the extent at which conventional nZVI synthesis methodologies can be applied in the field in order to act as a mechanism for the regeneration of nZVI-DE (following Cu recovery) for regeneration and reuse of the nZVI-DE. It is likely that aqueous chemical reduction methods (e.g. polyphenol or sodium borohydride reduction of aqueous iron onto DE surfaces) will be more appropriate than thermal chemical reduction (e.g. using H_2 or CO gas) or mechanical attrition (e.g. high speed ball milling) due its relative safety (being wet synthesis method) and low energy footprint (it can be performed at room temperature).

5. Conclusion

Herein DE has been investigated as a new matrix support for nZVI for the selective removal of Cu from AMD. Batch experiments were conducted using a range of different nZVI-DE concentrations (4.0-16.0 g/L) and over a time period of 672 hours. The following can be concluded:

1) nZVI can be loaded onto acid leached DE *via* a relatively simple batch chemical reduction process, with $FeCl_2.H_2O$ used as an iron source and $NaBH_4$ as the reducing agent. HRTEM indicated a relatively even distribution of nZVI on surface of the DE

and within its porous structure, with XPS and XRD confirming nZVI to be comprised of crystalline Fe^0 with a surface $Fe^0/(Fe^{2+}+Fe^{3+})$ stoichiometry of 0.20.

2) Cu recovery from AMD requires a relatively high concentration of nZVI-DE, with concentrations ≤4.0 g/L (4.0 g/L nZVI-DE equates to a dose of 0.104 g/L nZVI) imparting minimal changes to the solution electrochemistry (pH, Eh and DO) and metal/metalloid concentrations.

3) Exposure of nZVI-DE concentrations ≥12.0 g/L to the AMD resulted in the rapid and near total recovery of Cu from solution (>99.9 % removal within 1 h), despite the relatively low concentration of nZVI upon and within the DE (2.6 wt. %), likely *via* electrochemical cementation.

4) Minimal changes in the concentrations of numerous other metal and metalloid ions present in the AMD (namely: Na, Ca, Mg, K, Mn, and Zn) were recorded, which demonstrates the selectivity of nZVI-DE for redox amenable metals and metalloids.

5) Following near total removal of Cu from the aqueous phases during the initial stages of the reaction (<24 hrs) significant re-release back into the aqueous phase was recorded and attributed to the reactive exhaustion of the nZVI and ingress of atmospheric gases allowing recovery of system Eh, DO and pH. This phenomenon could potentially be engineered for the controlled release of the captured Cu.

Overall the results demonstrate nZVI-DE as highly selective for the rapid removal of Cu from AMD. The nanomaterial and the demonstrated uptake and release behaviour holds great promise as a next generation 'Precision Mining' tool for selective recovery of Cu from acidic wastewaters. Further work is required in order to determine both the hydraulic (e.g. colloidal stability, dynamic zeta potential) properties of the material and also its behaviour towards and

497 within biological systems. Moreover its ability to be regenerated (reloading the material with
498 nZVI) for repetitive use also needs to determined.

499

500 **5. Acknowledgement**

501 We would like to thank Mr Jeff Rowlands and Mr Marco Santonastaso from the School of
502 Engineering, Cardiff University for their technical support. We would also like to thank Mr
503 Phillip Goodman from Natural Resources Wales for his help organising the mine water
504 sample collection. We would also like to thank Dr Thomas Davies from the Cardiff Catalysis
505 Institute and the Cardiff Electron Microscopy Facility for the HRTEM-EDS analysis, Dr
506 David Morgan from the School of Chemistry, Cardiff University for the XPS and BET
507 surface area analysis and Dr Iain McDonald from the ELEMENT Facility within the School
508 of Earth Sciences for the ICP-MS analysis. This work was financially supported by the
509 Natural Environmental Research Council (grant number: NE/L013908/1) and the Camborne
510 School of Mines Trust.

511 **6. References**

512 Chao, J.T., Biggs, M.J., Pandit, A.S., 2014. Diatoms: a biotemplating approach to fabricating
513 drug delivery reservoirs. Expert Opinion on Drug Delivery. 11, 1687-1695.

514

515 Crane, R.A. Scott, T.B., 2014. The removal of uranium onto nanoscale zero-valent iron in
516 anoxic batch systems. Journal of Nanomaterials. 2014, 1-9.

517

518 Crane, R.A., Dickinson, M., Popescu, I.C., Scott, T.B., 2011. Magnetite and zero-valent iron
519 nanoparticles for the remediation of uranium contaminated environmental water. Water
520 Research. 45, 2931-2942.

521 Crane, R.A., Pullin, H., Macfarlane, J., Silion, M, Popescu, I.C., Andersen, M., Calen, V.,
522 Scott, T.B., 2015a. Field application of iron and iron-nickel nanoparticles for the ex situ
523 remediation of a uranium bearing mine water effluent. Journal of Environmental Engineering.
524 141, 241-259.
525
526 Crane, R.A., Pullin, H., Scott, T.B., 2015b. The influence of calcium, sodium and bicarbonate
527 on the uptake of uranium onto nanoscale zero-valent iron particles. Chemical engineering
528 Journal. 277, 252-259.
529
530 Crane, R.A., Scott, T.B., 2012. Nanoscale zero-valent iron: future prospects for an emerging
531 water treatment technology. Journal of Hazardous Materials. 211, 112-125.
532
533 Crane, R.A., Scott, T.B., 2014. The removal of uranium onto carbon-supported nanoscale
534 zero-valent iron particles. Journal of Nanoparticle Research. 16, 1-13.
535
536
537 EPA, 1996. Microwave assisted acid digestion of siliceous and organically based matrices,
538 URL: https://www.epa.gov/sites/production/files/2015-12/documents/3052.pdf. (Accessed
539 07/09/2017).
540
541
542 European Environment Bureau. 2000. The environmental performance of the mining industry
543 and the action necessary to strengthen European legislation in the wake of the Tisza-Danube
544 pollution. EEB Document no 2000/016. 32.
545

546 Hodson, R., 2016. Precision medicine. Nature. 537, S49.

547

548 Kay, C.M., Rowe, O.F., Rocchetti, L., Coupland, K., Hallberg, K.B., Johnson, D.B., 2013.
549 Evolution of Microbial "Streamer" Growths in an Acidic, Metal-Contaminated Stream
550 Draining an Abandoned Underground Copper Mine. Life. 3, 189-210.

551

552 Krook, J., Baas, L., 2013. Getting serious about mining the technosphere: a review of recent
553 landfill mining and urban mining research. Journal of Cleaner Production. 55, 1-9

554

555 Lee, S., Lee, K., Rhee, S., Park, J., 2007. Development of a new zero-valent iron zeolite
556 material to reduce nitrate without ammonium release, Journal of Environmental Engineering.
557 133, 6-12.

558

559 Lv, X., Xu, J., Jiang, G., Xu, X., 2011. Removal of chromium(VI) from wastewater by
560 nanoscale zero-valent iron particles supported on multiwalled carbon nano-tubes,
561 Chemosphere. 85, 1204–1209.

562

563 Noubactep, C., Caré S., Crane, R.A. 2012. Nanoscale metallic iron for environmental
564 remediation: prospects and limitations. Water Air Soil Pollution. 223, 1363-1382.

565

566 Oh, Y.J., Song, H., Shin, W.S., Choi, S.J., Kim, Y.-H., 2007. Effect of amorphous silica and
567 silica sand on removal of chromium(VI) by zero-valent iron, Chemosphere. 66, 858–865.

568

569 Pointon, C. R. & Ixer, R. A. 1980. Parys Mountain mineral deposit, Anglesey, Wales:
570 geology and ore mineralogy. Transactions of the Institution of Mining and Metallurgy. (Sect.

571 B" Appl. Earth Sci.), 89, 143-55.

572

573 Pojananukij, N., Wantala, K., Neramittagapong, S., & Neramittagapong, A. 2016.
574 Equilibrium, kinetics, and mechanism of lead adsorption using zero-valent iron coated on
575 diatomite. Desalination and Water Treatment, 57, 18475-18489.

576

577 Pojananukij, N., Wantala, K., Neramittagapong, S., Lin, C., Tanangteerpong, D., &
578 Neramittagapong, A. 2017. Improvement of As (III) removal with diatomite overlay
579 nanoscale zero-valent iron (nZVI-D): adsorption isotherm and adsorption kinetic studies.
580 Water Science and Technology: Water Supply, 17(1), 212-220.

581

582 Popescu, I.C., Filip, P., Humelnicu, D., Humelnicu, I, Scott, T.B., Crane, R.A., 2013.
583 Removal of uranium (VI) from aqueous systems by nanoscale zero-valent iron particles
584 suspended in carboxy-methyl cellulose. Journal of Nuclear Materials. 443, 250-255.

585

586 Pullin, H., Crane, R.A., Morgan, D.J., Scott, T.B., 2017. The effect of common groundwater
587 anions on the aqueous corrosion of zero-valent iron nanoparticles and associated removal of
588 aqueous copper and zinc. Journal of Environmental Chemical Engineering. 5, 1166–1173.

589

590 Qiu, X., Fang, Z., Liang, B., Gu, F., Xu, Z., 2011. Degradation of decabromodiphenyl ether
591 by nano zero-valent iron immobilized in mesoporous silica microspheres, Journal of
592 Hazardous Materials. 193, 70–81.

593

Ramos, M.A., Yan, W., Li, X-Q., Koel, B.E., Zhang, W-X., 2009. Simultaneous oxidation and reduction of arsenic by zero-valent iron nanoparticles: understanding the significance of the core-shell structure. The Journal of Physical Chemistry C. 113, 14591-14594.

Round, F.E., Crawford, R.M. Mann, D.G. 1990. The Diatoms: the Biology and Morphology of the Genera, Cambridge University Press. ISBN: 0521363187.

Sarikaya M. 1996. Biomimetics: materials fabrication through biology. Proceedings of the National Academy of Sciences. USA, 96, 14183-14185.

Scott T.B., Allen G.C., Heard P.J., Randell M.G., 2005. Reduction of U(VI) to U(IV) on the surface of magnetite, Geochimica et Cosmochimica Acta. 69, 5639–5646.

Scott, T B., Dickinson, M., Crane, R.A., Riba, O., Hughes, G. and Allen, G., 2010. The effects of vacuum annealing on the structure and surface chemistry of iron nanoparticles. Journal of Nanoparticle Research. 12, 2081-2092.

Scott, T.B., Popescu, I.C., Crane, R.A., Noubactep, C., 2011. Nano-scale metallic iron for the treatment of solutions containing multiple inorganic contaminants. Journal of Hazardous Materials. 186, 280-287.

Sheng G., Yang P., Tang Y., Hu Q., Li H., Ren X., Hu B., Wang X., Huang Y., 2016. New insights into the primary roles of diatomite in the enhanced sequestration of UO22+by zerovalent iron nanoparticles: An advanced approach utilizing XPS and EXAFS. Applied Catalysis B: Environmental. 193, 189–197

Stefaniuk, M., Oleszczuk, P., Ok, Y.S., 2016. Review on nano zerovalent iron (nZVI): from synthesis to environmental applications. Chemical Engineering Journal, 287, 618-632.

USGS (2012) https://minerals.usgs.gov/minerals/pubs/commodity/diatomite/mcs-2013-diato.pdf (Accessed 07/09/2017)

WHO (2011) Guidelines for Drinking-water Quality. Forth Edition. ISBN: 978 92 4 154815 1. URL: http://www.who.int/water_sanitation_health/publications/2011/dwq_guidelines/en/ (Accessed 07/09/2017)

Xi, Y., Megharaj M., Naidu R., 2011. Dispersion of zerovalent iron nanoparticles onto bentonites and use of these catalysts for orange II decolourisation, Applied Clay Science. 53, 716–722.

Yunfei, X., Mallavarapu, M., Naidu, R., 2010. Reduction and adsorption of Pb 2+ in aqueous solution by nano-zero-valent iron—a SEM, TEM and XPS study. Materials Research Bulletin. 45, 1361-1367

Towards “Precision Mining” of wastewater: selective recovery of Cu from acid mine drainage onto diatomite supported nanoscale zerovalent iron particles

R. A. Crane[1,2] and D. J. Sapsford[1]*

[1] School of Engineering, Cardiff University, Queen's Building, The Parade, Cardiff, CF24 3AA. United Kingdom

[2] Camborne School of Mines, University of Exeter, Penryn Campus, Penryn, Cornwall, TR10 9FE. United Kingdom

* Corresponding author: cranera@cardiff.ac.uk

Research highlights

- Precision Mining of a metal from wastewater reported for the first time
- Mechanism of Cu removal onto nZVI-DE via cementation with nZVI
- nZVI-DE selective for Cu removal despite presence of other metals (Na, Ca, Mg, Mn, Zn, etc.)
- Near-total removal of Cu ions followed by redissolution after nZVI reactive exhaustion
- Re-release mechanism could be harnessed as new technique to concentrate Cu